Adv. Manuf. (2017) 5:251–260
DOI 10.1007/s40436-017-0188-3

Surface texture formation in precision machining of direct laser deposited tungsten carbide

Szymon Wojciechowski[1] · Zbigniew Nowakowski[1] · Radomir Majchrowski[1] · Grzegorz Królczyk[2]

Received: 29 September 2016 / Accepted: 26 July 2017 / Published online: 6 September 2017

Abstract This paper focuses on an analysis of the surface texture formed during precision machining of tungsten carbide. The work material was fabricated using direct laser deposition (DLD) technology. The experiment included precision milling of tungsten carbide samples with a monolithic torus cubic boron nitride tool and grinding with diamond and alumina cup wheels. An optical surface profiler was applied to the measurements of surface textures and roughness profiles. In addition, the micro-geometry of the milling cutter was measured with the application of an optical device. The surface roughness height was also estimated with the application of a model, which included kinematic-geometric parameters and minimum uncut chip thickness. The research revealed the occurrence of micro-grooves on the machined surface. The surface roughness height calculated on the basis of the traditional kinematic-geometric model was incompatible with the measurements. However, better agreement between the theoretical and experimental values was observed for the minimum uncut chip thickness model.

Keywords Surface texture · Precision machining · Tungsten carbide · Direct laser deposition (DLD)

Abbreviations

a_e	Radial depth of cut, mm
a_p	Axial depth of cut, mm
D	Tool diameter, mm
f_z	Feed per tooth, μm/tooth
f_{z_cr}	Feed per tooth critical value, mm/tooth
h	Uncut chip thickness, mm
h_{max}	Maximum uncut chip thickness, mm
h_{min}	Minimum uncut chip thickness, mm
k	Constant of proportionality in the expression of minimum uncut chip thickness
k_f	Fracture ratio coefficient
l_f	Evaluation length, mm
P_{A0}	Total number of pixels for the entire image
P_{Ai}	Total number of pixels for the fractured areas
R_a	Average surface roughness height, μm
R_k	Core roughness depth, μm
r_n	Cutting edge radius, mm
R_{pk}	Mean height of the peaks on the roughness core profile, μm
R_{tB}	Theoretical height of surface roughness including minimum uncut chip thickness, μm
R_{zt}	Theoretical height of surface roughness, μm
R_z	Surface roughness height, μm
r_ε	Tool corner radius, mm
t_s	Cutting time, min
v_c	Cutting speed, m/min
v_f	Feed rate, mm/min
γ_o	Orthogonal rake angle, (°)
φ	Positioning angle corresponding to maximum uncut chip thickness, (°)

1 Introduction

The excellent properties of tungsten carbides, such as high hardness, high wear resistance, and good toughness enable its wide application in many industries. Tungsten carbides

✉ Grzegorz Królczyk
g.krolczyk@po.opole.pl

[1] Faculty of Mechanical Engineering, Poznan University of Technology, Piotrowo 3, Poznan, 60-965 Poznan, Poland

[2] Opole University of Technology, Proszkowska 76, 45-758 Opole, Poland

have been widely used in the production of cutting tools, molds, dies, as well as wear resistant parts, for example, dental burs applied in dental restorations, tool bits intended for cutting and rock drilling, and ore crushing equipment [1]. Another area of application is the optical industry, including the manufacturing of optical inserts in ceramic powder injection molding and glass injection molding, as well as advanced optical transmission equipment [2].

The wide application of cemented carbides in the production of precision parts imposes restrictive requirements related to low surface roughness and high dimensional accuracy [3]. Therefore, these materials are usually manufactured with the application of powder metallurgy technology, and then subjected to grinding with diamond wheels. However, the application of grinding results in extensive machining-induced cracks and damages to the work material. In order to remove these faults and improve surface roughness, lapping and polishing processes with the use of fine diamond abrasives can be employed [4]. Metrological analysis in the context of functional properties have been discussed in Refs. [5–7]. Nevertheless, these processes can cause a decline in form accuracy and increase in machining time and cost [8].

A novel technology applied to the finishing of brittle and hard materials is ultraprecision machining. According to Stephenson et al. [9], this technology significantly reduces the number of cracks and damages on the machined surface, and also improves its geometrical accuracy. Ultraprecision machining is based on the Bifano model [10], related to the brittle-ductile transition during chip formation. This model states that if the maximum chip thickness selected in machining is less than the critical cut depth that involves cracking of the material, then the machining will occur in the ductile regime, i.e., without residual cracks on the formed surfaces. Practically, ultraprecision machining with the application of tools with defined geometry is feasible when the ratio of the cutting edge radius to the uncut chip thickness is greater than unity [11]. For example, Liu and Li [12] conducted grooving tests of tungsten carbide samples, with the use of cubic boron nitride (CBN) inserts with cutting edge radius $r_n = 5.8$ μm. The results showed that the transition from the brittle to ductile cutting mode occurred when the uncut chip thickness $h < 2.5$ μm. The next research conducted by Liu et al. [13] included milling tests of tungsten carbide P30 with the application of an ultraprecision machine tool, CBN cutter with cutting edge radius $r_n = 3.4$ μm and uncut chip thickness equal to 0.8 μm. The research revealed that during ductile mode milling of tungsten carbide, the average surface roughness R_a values were below 0.2 μm and independent of cutting speed and tool wear. Ultraprecision diamond turning of brittle reaction-bonded silicon carbide (RB-SiC) was carried out by Yan et al. [14]. They stated that the mechanism for material removal involved ductile cutting, cleavage cracking, and grain dislodgement. Furthermore, the surface roughness was affected by the occurrence of fractures, the intensity of which depended on the feed rate value. Overall, ultraprecision machining has many advantages; however, it requires the accurate compensation of machining errors [15] and application of expensive machine tools characterized by high rigidity, damping, and precision of control.

Direct laser deposition (DLD) is a developing technology that can be alternatively applied to the manufacture of tungsten carbides for individual or small-quantity production. The DLD method enables the production of metallic powder prototypes by a layer manufacturing method [16, 17]. The primary objective of DLD technology is the regeneration of machine parts or machine parts manufacturing with improved surface layer properties, e.g., higher corrosion, erosion, and abrasion resistance. Unfortunately, parts produced by DLD technology are characterized by the occurrence of porosity and thus have unsatisfactory geometric accuracy, as well as surface roughness [18, 19]. Therefore, post-process machining is required for the surface quality improvement.

References [20–22] have revealed that precision milling of DLD tungsten carbides with the application of CBN end mills is feasible and increases surface quality. However, the obtained surface roughness was independent of the feed per tooth value and characterized by the appearance of micro-grooves, which substantially affected the growth of the surface roughness.

Another significant problem occurring during machining of the hard-to-cut materials with the selection of low feed per tooth values (e.g., precision and ultraprecision machining) is the growth of surface roughness height. According to Refs. [23, 24], this phenomenon can be caused by plastic deformation in the primary shear zone and post-machining elastic recovery of this surface. Furthermore, Rahman et al. [25] stated that surface generation mechanisms were also significantly affected by the ratio of uncut chip thickness to cutting edge radius. Therefore, in order to accurately estimate the surface roughness height during cutting with low feeds, the Brammertz model can be applied [23]. This kind of approach includes the feed rate, corner radius, cutting edge radius, and minimum uncut chip thickness.

The state of the art presented above shows that problems of surface texture formation during machining of hard-to-cut materials need further studies. Therefore, this paper presents a surface texture analysis during precision machining of DLD tungsten carbide. Precision machining is an advanced manufacturing technology that can be applied in relation to hard metallic materials with complex geometries at high precision of machined surfaces [26, 27]. According to Ref. [28], it bridges the gap between the

conventional machining and ultraprecision machining. Thus, the recognition of phenomena and process input parameters affecting machined surface quality is of high importance.

The present experiment included milling tests of tungsten carbide samples with a monolithic CBN tool and grinding with diamond and alumina cup wheels. The machined surfaces were inspected with an optical surface profiler. In addition, the micro-geometry of the milling cutter was measured with the application of an optical device. The surface roughness height was also estimated with the application of a model that included kinematic-geometric parameters and minimum uncut chip thickness. The measurements involved the determination of R_a and R_z profile parameters, because they enable the validation of the applied surface roughness 2D models. However, in order to recognize the machining marks and micro-grooves (i.e., k_f), 3D surface textures were determined. In addition, the R_{pk} and R_k parameters were selected in order to evaluate the machined surface's adherence and abrasion resistance.

2 Experimental details

2.1 Machining tests

The investigated samples with dimensions of 73 mm × 23 mm (see Fig. 1) were manufactured by the plasma SYSTEM company with the application of DLD technology. The WC-NiFeCr samples contained 52% WC powder (mass fraction) and 48% NiFeCr powder (mass fraction). The size of the WC grains was equaled approximately to 40–100 μm. Symmetrical face milling and plane grinding tests were conducted on the samples. Both experiments were carried out with the application of coolants. A one-toothed CBN monolithic torus end mill was applied as a milling tool. Its geometry was as follows: diameter $D = 8$ mm; corner radius $r_\varepsilon = 200$ μm; orthogonal rake angle $\gamma_o = -5°$. The milling experiments were carried out on the rigid five-axis DECKEL MAHO model DMU 60monoBLOCK milling center.

The plane grinding of samples was conducted on FUM SPC 20B grinding machine with the application of fine-grained diamond and alumina cup wheels, with diameter $D = 200$ mm. The grit sizes of the applied grinding wheels were 106–125 μm in the case of diamond wheels and 250–300 μm in the case of alumina wheels. The experimental design is presented in Table 1.

2.2 Surface texture measurements

The surface textures were measured using an optical surface profiler (Veeco NT 1100). The measurements were made with 5.1-fold magnification. The scanning area was 0.9 mm × 1.2 mm and the distance of vertical points was 1.65 μm. The acquired signals were processed in Veeco Vision 32 software.

In order to indicate the extent of microfractures on the machined surfaces, the fracture ratio coefficient k_f was adapted from Ref. [14]. Its value was calculated on the basis of the measured surface textures with the application of Photoshop® software. As shown in Fig. 2, by counting the total number of pixels for the fractured areas (P_{Ai}, $i = 1, 2, 3, \cdots$) and that of the entire image (P_{A0}), k_f can be formulated from the following equation:

$$K_f = \frac{\sum_{i=0}^{\infty} P_{Ai}}{P_{A0}}. \quad (1)$$

2.3 Surface roughness estimation

The 2D surface roughness parameters were evaluated with the application of a portable stylus profiler Hommelwerke T500, equipped with T5E head and Turbo DATAWIN software. The measurements were carried out parallelly to the feed motion direction, including six repetitions for each investigated surface. The evaluation length for the milled surfaces was 4.8 mm, while in case of ground surfaces, $l_f = 15$ mm. As a result of measurements, the following surface roughness parameters were determined: R_a, R_z, R_{pk}, and R_k.

In order to characterize the surface formation during precision machining of tungsten carbides, the Brammertz model was adapted. This approach considers the kinematic-geometric parameters, as well as the plastic-elastic deformations of the work material during cutting with very low

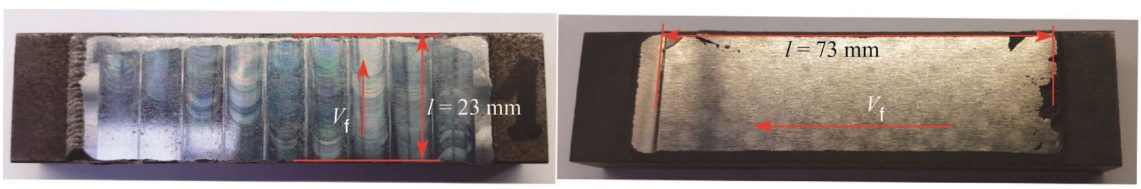

(a) After precision milling **(b)** After grinding

Fig. 1 Tungsten carbide samples

Table 1 Design of experiments

Precision milling test				Plane grinding tests with diamond and alumina cup wheels			
f_z/(μm · tooth^{-1})	v_c/(m · min^{-1})	a_e/mm	a_p/μm	v_f/(m · min^{-1})	v_t/(mm · min^{-1})	v_c/(m · s^{-1})	a_p/μm
5	30	4	20	16	131	25	5
20	30	4	20				
40	30	4	20				

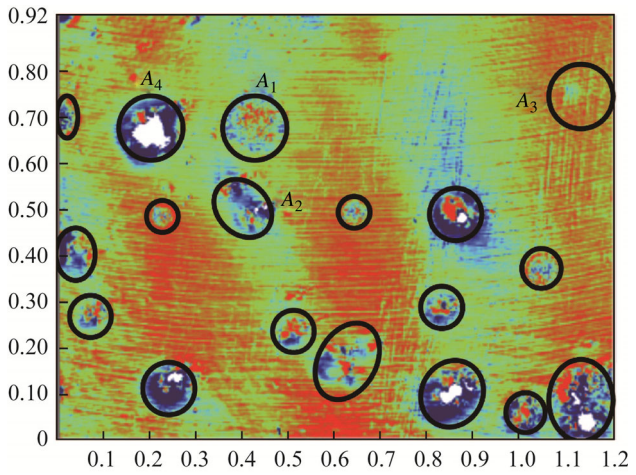

Fig. 2 Scheme of method applied for calculation of the fracture ratio (surface after precision milling)

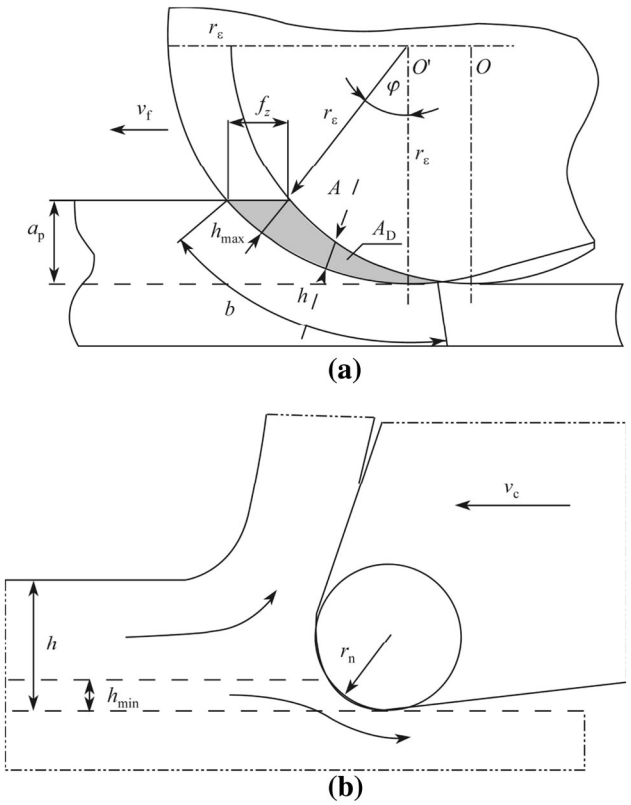

Fig. 3 Chip formation model including minimum uncut chip thickness during arc-shaped immersion of tool into the workpiece

uncut chip thicknesses ($h \approx h_{\min}$). According to Ref. [23], the theoretical height of the surface roughness during machining with a one-toothed tool is expressed by the following equation

$$R_{tB} = \frac{f_z^2}{8r_\varepsilon} + \frac{h_{\min}}{2}\left(1 + \frac{r_\varepsilon h_{\min}}{f_z^2}\right). \quad (2)$$

In order to solve Eq. (2), the determination of minimum uncut chip thickness value $h_{\min}$ is required. The $h_{\min}$ (see Fig. 3) depends mainly on the cutting edge radius r_n and mechanical properties of the work material (as hardness and flow stress).

Therefore, according to Ref. [29], the minimum uncut chip thickness value can be calculated from the expression

$$h_{\min} = kr_n. \quad (3)$$

According to Ref. [12], the value of k is equal to 0.428 during ultraprecision turning of tungsten carbide with CBN inserts.

In order to determine the cutting edge radius r_n of the CBN end mill, measurements of the tool's microgeometry with the application of the Alicona IF Edgemaster optical device were carried out. Analyses were conducted for the new tool (cutting time $t_s = 0$), and for the worn tool (after cutting time $t_s = 9$ min).

The application of Eq. (2) also enables the calculation of feed per tooth critical value f_{z_cr}, corresponding to minimal surface roughness height. The f_{z_cr} can be determined on the basis of the following expression [23]

$$f_{z\_cr} = \sqrt{2h_{\min}r_\varepsilon}. \quad (4)$$

From the investigation, the critical feed per tooth f_{z_cr} was obtained as 22 μm/tooth. During the face milling carried out in conditions of an arc-shaped immersion of tool into the work material ($a_p \leqslant r_\varepsilon$), the maximal uncut chip thickness (for the selected cutting parameters) $h_{\max}$ can be expressed by the equation

$$h_{\max} = r_\varepsilon + f_z \sin\varphi - \sqrt{r_\varepsilon^2 - f_z^2 \cos^2\varphi}. \quad (5)$$

The φ angle corresponding to $h_{\max}$ value (see Fig. 3) can be calculated from the expression developed on the basis of the trigonometric dependencies

$$\varphi = \arctan\left(\frac{\sqrt{a_p(2r_\varepsilon - a_p)} - f_z}{r_\varepsilon - a_p}\right). \quad (6)$$

The present calculations reveal that in the investigated range, the maximum uncut chip thicknesses were $h_{\max} \geqslant 2.1$ μm.

3 Results and discussions

Figures 4–6 depict surface textures obtained after milling and grinding with the application of diamond and alumina wheels.

The surfaces after milling reveal the appearance of micropits, which are seen for all investigated feed per tooth values f_z. An analysis of the fracture ratio k_f (see Fig. 7), shows that the intensity of micropits' occurrence on the milled surface decreases with the growth of the parameter f_z. The dimensions of these microgrooves exceed 100 μm; therefore, they are larger than WC grains. The occurrence of micropits is caused by the dislodgement of WC grain fractions from the surface by the tool tip. This phenomenon depends mainly on the bonding strength at the grain boundaries. However, it can be also related to the appearance of the work material's defects, as micropores which were formed during the DLD process [18, 19].

The inspection of surface textures after milling reveals the occurrence of feed marks. Thus, the mechanism of material removal during milling is affected by the plastic-elastic deformation of the workpiece.

The micropits can be also observed on surfaces formed during grinding with the application of diamond wheels. However, the agglomeration of micropits is in this case significantly lower than that obtained for the milled surfaces. This observation is confirmed by the mean value of the fracture ratio equal to 0.019. In contrast, the k_f values for the milled surfaces are always higher than 0.03.

In case of samples ground with the application of alumina wheels (see Fig. 6), fracture-free surfaces were formed ($k_f = 0$). This suggests that the material removal was based mainly on fracture of WC grain fractions, which can be obtained by the application of alumina grinding wheels with the coarser grit size (250–300 μm) than that for the diamond grinding wheel (106–125 μm). The increase of grit size causes a growth in the minimum uncut chip thickness value (according to Eq. (3)), and thus the compressive stresses on the material being cut. Consequently, it facilitates the separation of hard WC grain fractions and leads to the elimination of fractions' dislodgement. It should be noted that ground surface quality improvement together with the growth in the grit size was also observed during the ultraprecision grinding of polycrystalline silicon carbide with the application of diamond wheels with grit sizes of 15 μm and 25 μm [8].

Figure 8 depicts the comparison of cutting edge profiles and images obtained for the new and worn tool. It can be observed that for the new cutter, the mean value of the cutting edge radius (r_n) is 2.9 μm. In the case of measurements carried out on the worn tool, the mean value of the cutting edge radius (r_n) increased to 145 μm. The considerable growth in the r_n value was caused by the abrasive effect of the hard tungsten carbide particles against the cutting edge, which consequently induced the cutter's mass loss and the modification of the cutting edge's shape (see Figs. 8b, d). The worn tool's microgeometry measurements were made on a rectilinear section of the cutting edge. Nevertheless, during the arc-shaped immersion of the tool into the work material, this area is not directly involved in the formation of the surface profile. Therefore, in order to estimate the minimum uncut chip thickness and theoretical surface roughness during milling of tungsten carbide, only the cutting edge radius value obtained for the new tool ($r_n = 2.9$ μm) was taken into consideration. As a result of the calculations, the obtained minimum uncut chip thickness was $h_{\min} = 1.2$ μm. Consequently, the estimated $h_{\min}$ value was applied to the calculation of surface roughness height, according to Eq. (2), in the range of investigated feed per tooth values.

Figure 9 presents the comparison of surface roughness parameter R_z as a function of feed, measured with the surface profiler and estimated on the basis of traditional kinematic-geometric model ($R_{zt} = f_z^2/8r_\varepsilon$), and the Brammertz model (Eq. (2)). It was observed that surface roughness calculated on the basis of the traditional model varied significantly from the measurement, both in quantitative and qualitative aspects. However, in case of the Brammertz model, a considerably better agreement between the calculations and measurements is seen. The Brammertz model includes both kinematic-geometric factors and elastic-plastic phenomena that occur during cutting with very low uncut chip thicknesses. According to Eq. (4), the reduction of feed per tooth below a certain critical value (f_{z_cr}) leads to an increase in the surface roughness height. This dependency can be seen in Fig. 9, in the range of feed per tooth $f_z < 20$ μm/tooth, which suggests that during precision milling of direct laser deposited tungsten carbide, the surface texture is formed with the contribution of elastic-plastic phenomena, occurring in the range of minimum uncut chip thickness. Nevertheless,

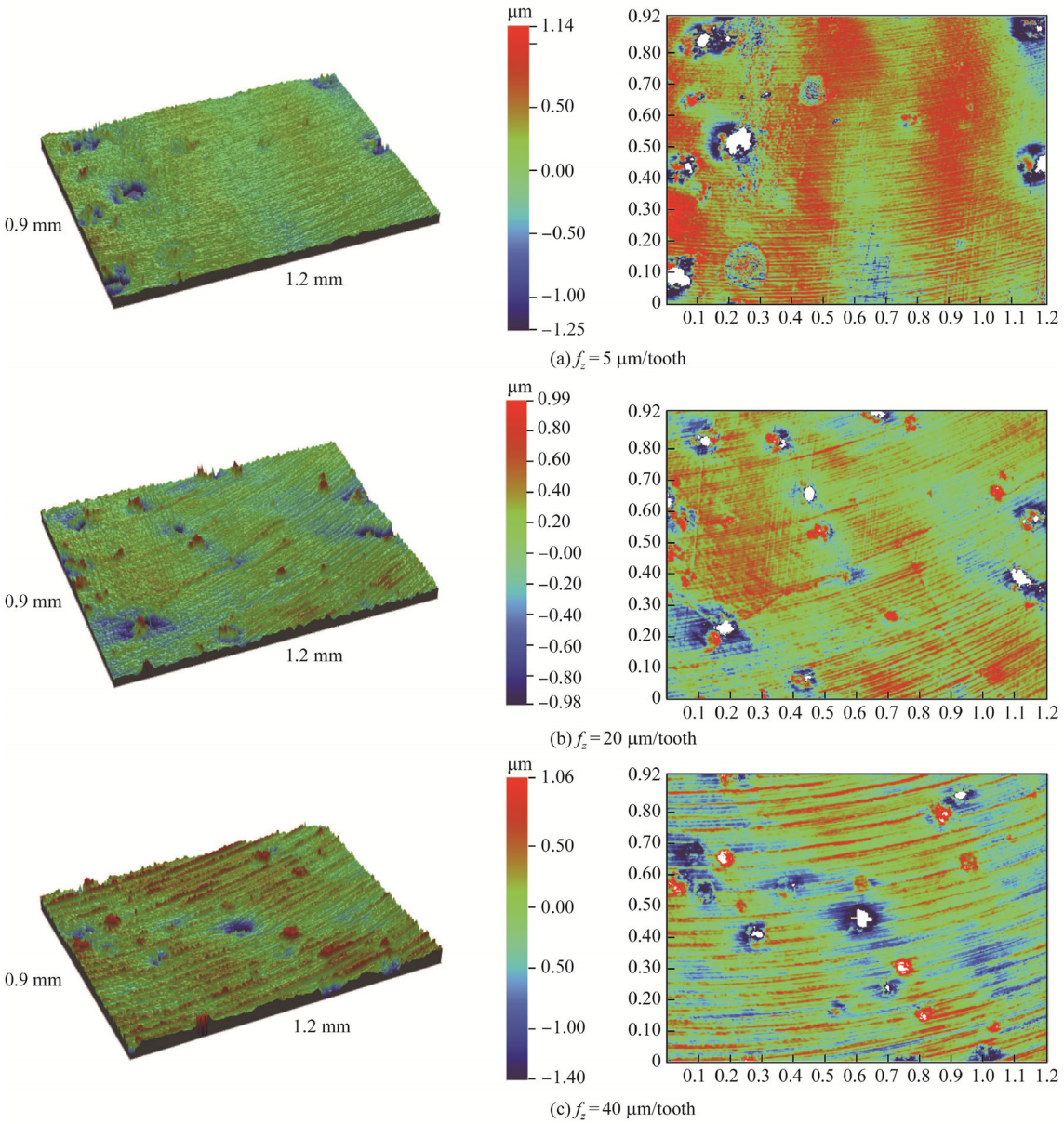

Fig. 4 Surface textures of tungsten carbides after precision milling

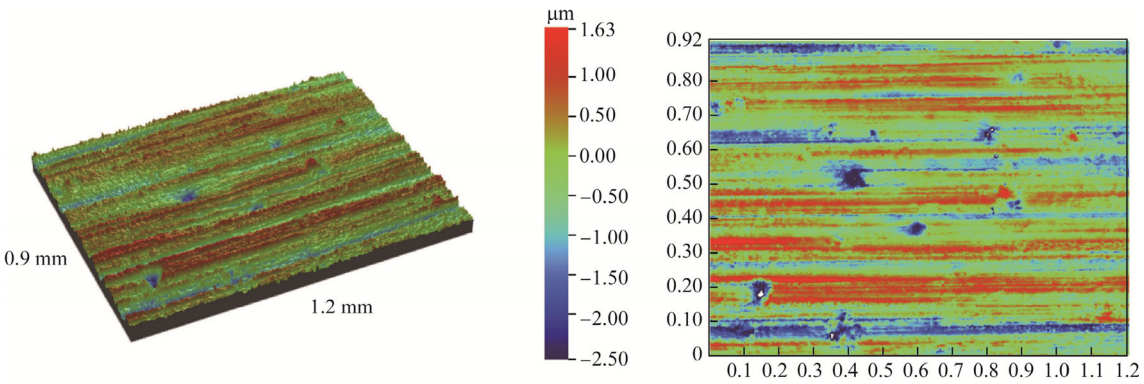

Fig. 5 Surface textures of tungsten carbides after grinding with diamond wheel

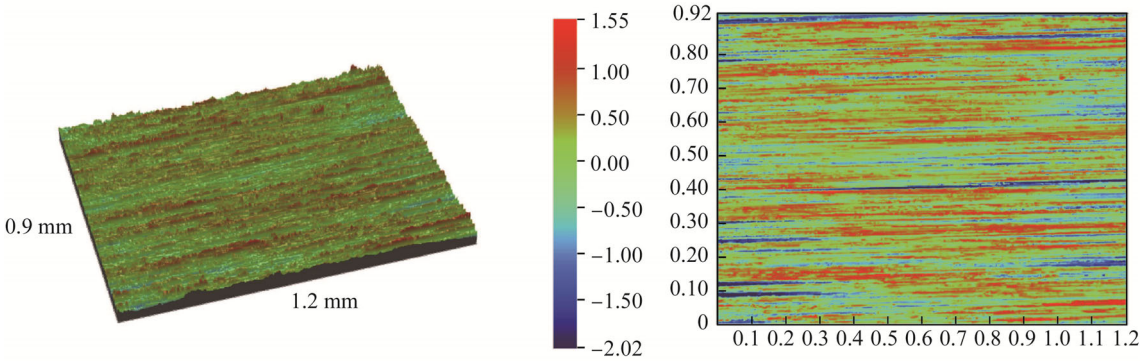

Fig. 6 Surface textures of tungsten carbides after grinding with alumina wheel

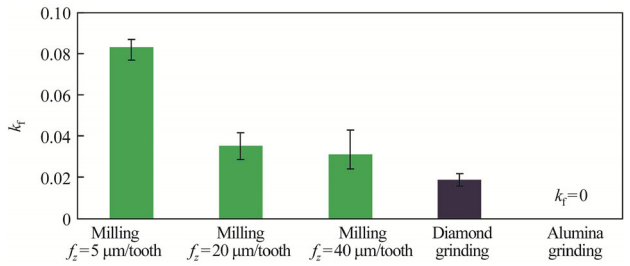

Fig. 7 Comparison of fracture ratio after machining of tungsten carbide

some discrepancies between the measured and modeled (on the basis of Eq. (2)) surface roughness heights are found. These differences can result from the inaccuracy of the h_{min} estimation, as well as the WC grain fractions' dislodgement mechanism, which leads to the formation of micropits on the machined surface.

Figures 10 and 11 compare the surface roughness parameters R_a and R_z after milling (f_z = 20 μm/tooth) and grinding. It can be seen that the lowest mean values of R_a and R_z parameters are found for the milled samples, then

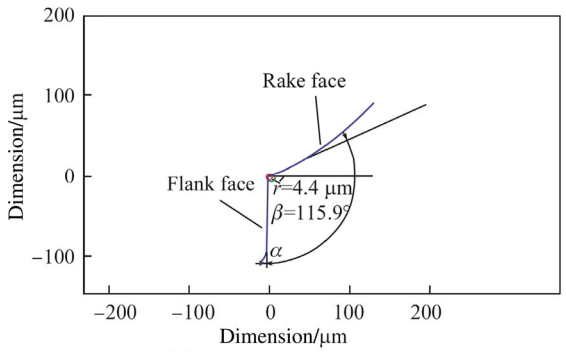

(a) Profile of the new tool

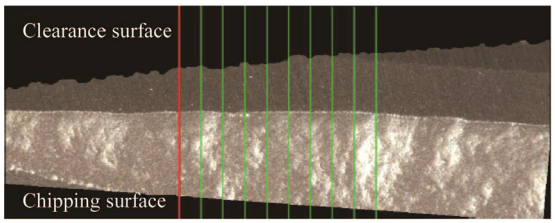

(b) Image of the new tool

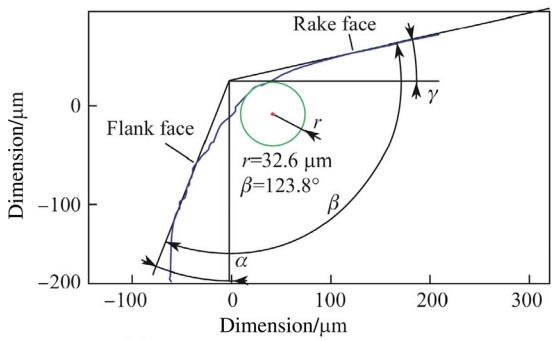

(c) Profile of tool after t_s = 9 min

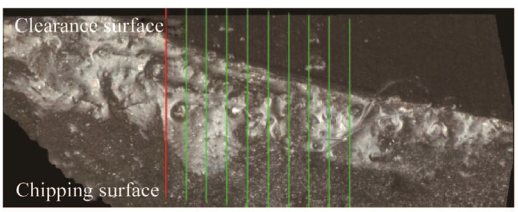

(d) Image of tool after t_s = 9 min

Fig. 8 CBN tool's working part microgeometry

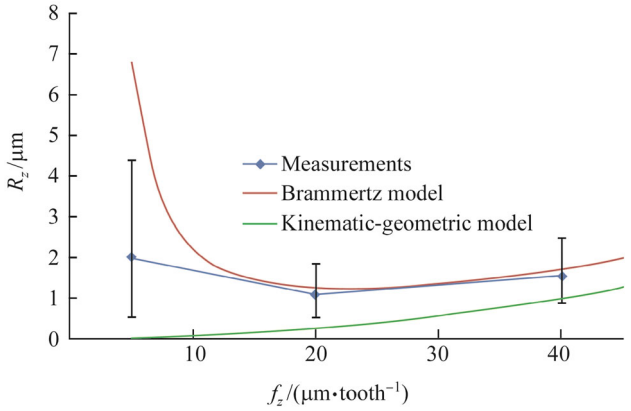

Fig. 9 Profile roughness height after precision milling in function of feed per tooth (WC DLD; End mill CBN; $D = 8$ mm; $a_p = 0.02$ mm; $r_\varepsilon = 0.2$ mm; $r_n = 2.9$ μm)

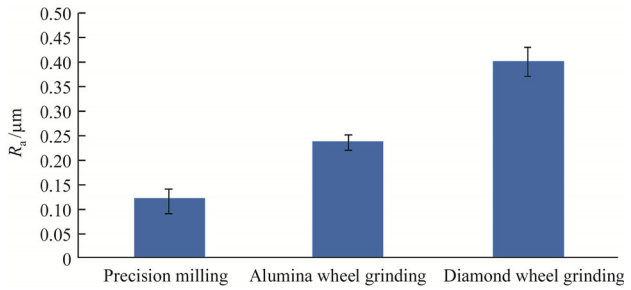

Fig. 10 Profile roughness R_a after precision milling and grinding

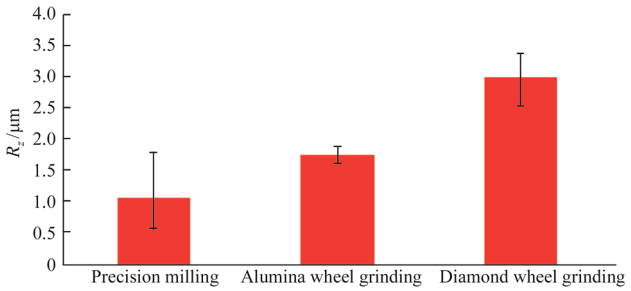

Fig. 11 Profile roughness R_z after precision milling and grinding

for the ground ones with the application of an alumina wheel, and finally, for samples ground with a diamond wheel. It should be noted that, despite the appearance of micropits on the machined surface, the milling process enables the achievement of the lowest surface roughness. This can be attributed to the application of a sharp CBN tool ($r_n = 2.9$ μm), which reduces the minimum uncut chip thickness value and thus, surface roughness height (according to Eq. (2)). In the case of grinding, the grit radius values are higher than 50 μm, which leads to the significant reduction (or even elimination) of micropit formation on the machined surface, but on the other hand, it induces the increase in surface roughness.

One of DLD tungsten carbides' potential applications is the regeneration of worn machine parts and manufacturing of spare parts for the aerospace and ship-building industries. Therefore, the performance and tribological properties of the interfering surfaces are of great interest. In order to evaluate these properties, the material ratio of the profile (the Abbot-Firestone curve) was taken into account. Figure 12 presents the comparison of the mean height of the peaks on the roughness core profile R_{pk} and the core roughness depth R_k after the investigated machining methods. It can be observed that milled surfaces are characterized by lower R_{pk} and R_k values than those obtained after grinding. This observation is favorable for the milling process, because low R_{pk} and R_k values indicate good surface adherence and abrasion resistance, as well as predisposition to work in high-stress conditions [30]. In addition, these dependencies are confirmed by the material ratio of the profile curves, which have a progressive character during milling and follow a regressive course after grinding (see Figs. 13, 14).

4 Conclusions

This paper focused on a surface texture analysis during machining of direct laser deposited tungsten carbide. The experiment included precision milling of tungsten carbide samples with a monolithic CBN tool and grinding with diamond and alumina cup wheels. On the basis of this research, the following conclusions were formulated:

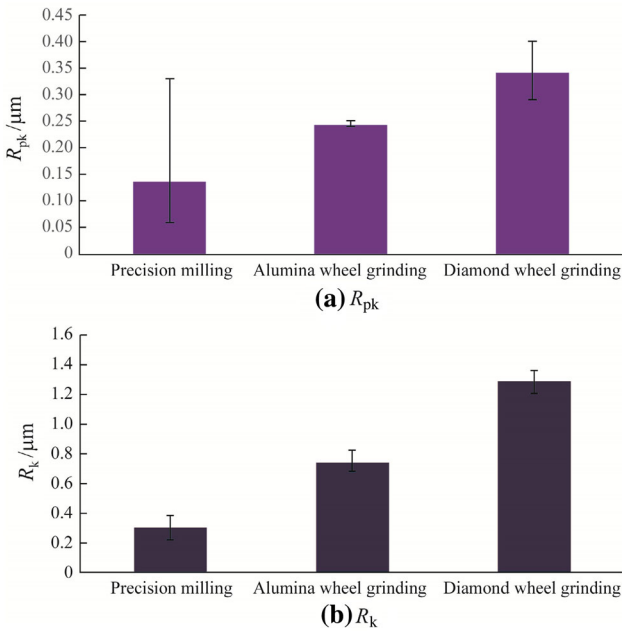

Fig. 12 Material ratio of the profile parameters after precision milling and grinding

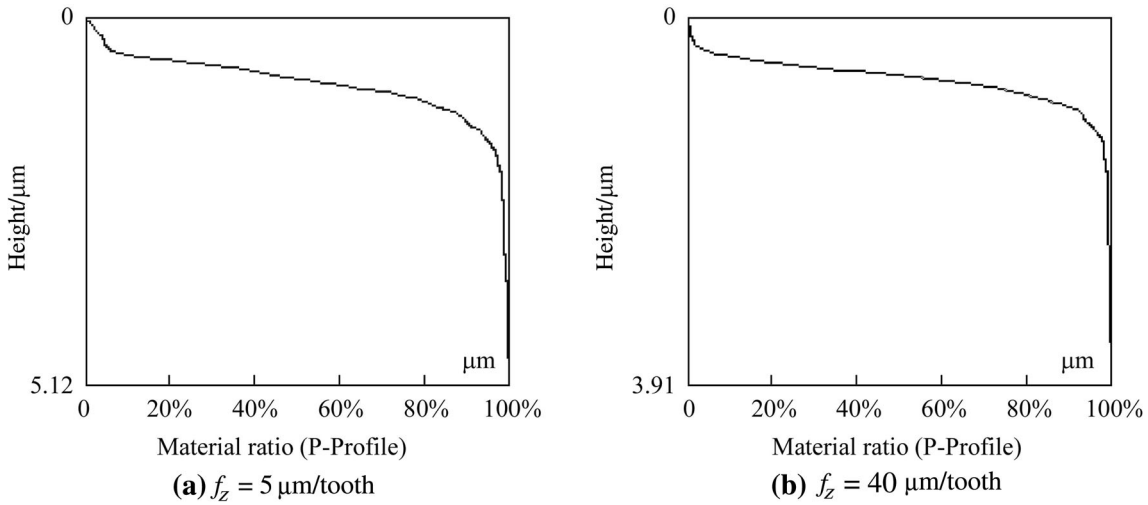

Fig. 13 Abbot-Firestone curve after precision milling

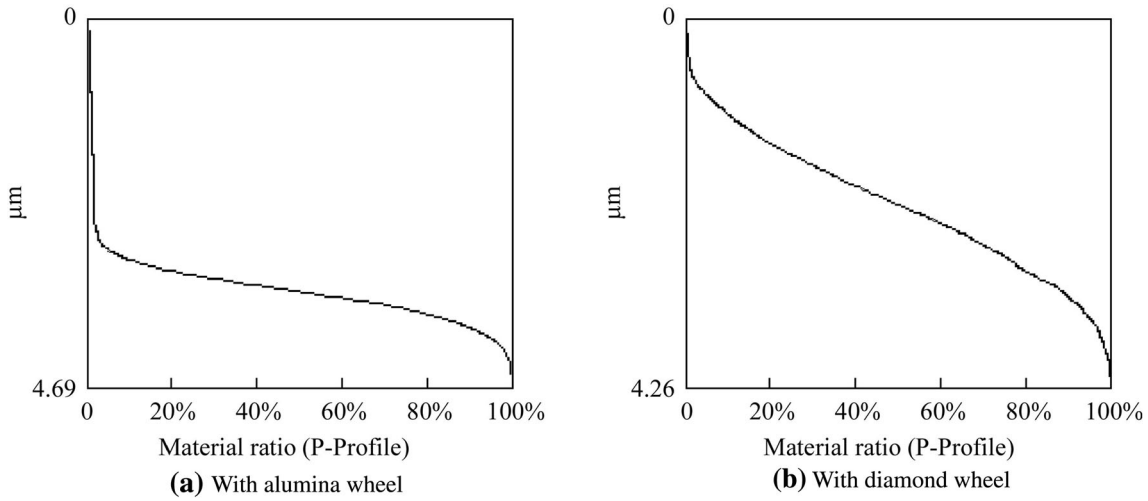

Fig. 14 Abbot-Firestone curve after grinding

(i) The surface texture formation during machining of direct laser deposited tungsten carbide is affected by the kinematic-geometric factors and elastic-plastic phenomena that occur during cutting with very low uncut chip thicknesses. In addition, the dislodgement mechanism of tungsten carbide grain fractions can be observed after CBN milling and grinding with a diamond wheel. The dislodgement mechanism is responsible for the appearance of micropits on the machined surface.

(ii) The highest extent of micropits on the machined surface is found for milled samples with a feed per tooth value f_z = 5 μm/tooth. In this case, the fracture ratio k_f was over four-fold higher than that obtained after grinding with a diamond wheel. Furthermore, the samples ground with the application of alumina wheels were fracture-free ($k_f = 0$). This suggests that micropit formation can be influenced by the cutting edge radius (relatively grit size during grinding). However, this problem requires further studies.

(iii) The lowest surface roughness parameter values (R_a, R_z, R_{pk}, R_k) were obtained for the milled samples. The differences between R_a and R_z values were up to 208% for R_a and 200% for R_z in comparison to samples after grinding with a diamond wheel. However, in the case of samples ground with the alumina wheel, the discrepancies were approximately 84% for R_a and 80% for R_z. Additionally, the milled surfaces have better adherence and abrasion resistance than ground samples, which is confirmed by the lower R_{pk} and R_k values.

Acknowledgements The research was supported by the project 02/22/DSMK/1228, 2015.

References

1. Han D, Mecholsky JJ Jr (1990) Fracture analysis of cobalt-bonded tungsten carbide composites. J Mater Sci 25:4949–4956
2. Yin L, Spowage AC, Ramesh K et al (2004) Influence of microstructure on ultraprecision grinding of cemented carbides. Int J Mach Tools Manuf 44:533–543
3. Krolczyk GM, Legutko S (2014) Experimental analysis by measurement of surface roughness variations in turning process of duplex stainless steel. Metrol Meas Syst XXI 4:759–770
4. Novak M, Naprstkova N, Jozwik J (2015) Analysis of the surface profile and its material share during the grinding Inconel 718 alloy. Adv Sci Technol Res J 9(26):41–48
5. Jun S, Kochan O (2014) Investigations of thermocouple drift irregularity impact on error of their inhomogeneity correction. Meas Sci Rev 14(1):29–34
6. Glowacz A, Glowacz Z (2016) Diagnostics of stator faults of the single-phase induction motor using thermal images, MoASoS and selected classifiers. Measurement 93:86–93
7. Krolczyk GM, Krolczyk JB, Maruda RW et al (2016) Metrological changes in surface morphology of high-strength steels in manufacturing processes. Measurement 88:176–185
8. Yin L, Vancoile EYJ, Lee LC et al (2004) High-quality grinding of polycrystalline silicon carbide spherical surfaces. Wear 256:197–207
9. Stephenson DJ, Vaselovac D, Manley S et al (2001) Ultra-precision grinding of hard steels. Precis Eng 25(4):336–345
10. Bifano TG, Dow TA, Scattergood RO (1991) Ductile-regime grinding: a new technology for machining brittle materials. ASME J Eng Ind 113(5):184–189
11. Liu K, Li XP (2011) Modelling of ductile cutting of tungsten carbide. Trans NAMRI/SME XXIX:251–258
12. Liu K, Li XP (2011) Ductile cutting of tungsten carbide. J Mater Process Technol 113:348–354
13. Liu K, Li XP, Rahman M et al (2003) CBN tool wear in ductile cutting of tungsten carbide. Wear 255:1344–1351
14. Yan J, Zhang Z, Kuriyagawa T (2009) Mechanism for material removal in diamond turning of reaction-bonded silicon carbide. Int J Mach Tools Manuf 49:366–374
15. Liu X, Zhang X, Fang F et al (2016) Identification and compensation of main machining errors on surface form accuracy in ultra-precision diamond turning. Int J Mach Tools Manuf 105:45–57
16. Banerjee R, Collins PC, Genc A (2003) Direct laser deposition of in situ Ti-6Al-4V-TiB composites. Mater Sci Eng A 358:343–349
17. Fearon E, Watkins KG (2004) Optimisation of layer height control in direct laser deposition. In: 23th international congress on applications of lasers & electro–optics (ICALEO 2004)
18. Simchi A, Pohl H (2003) Effects of laser sintering processing parameters on the microstructure and densification of iron powder. Mater Eng A 359:119–128
19. Liu FR, Zhang Q, Zhou WP et al (2012) Micro scale 3D FEM simulation on thermal evolution within the porous structure in selective laser sintering. J Mater Process Technol 212:2058–2065
20. Wojciechowski S, Twardowski P, Chwalczuk T (2014) Surface roughness analysis after machining of direct laser deposited tungsten carbide. In: International conference on metrology properties of engineering surfaces 2014:12018−12025(8)
21. Twardowski P (2011) Surface roughness analysis in milling of tungsten carbide with CBN cutters. Metrol Meas Syst XVIII 1:105–114
22. Wstawska I (2015) The influence of technological parameters on surface texture of DLD cemented tungsten carbide after grinding. Arch Mech Technol Mater 35:33–40
23. Grzesik W (2017) Advanced machining processes of metallic materials: theory, modelling and applications. Elsevier, Oxford
24. Schultheiss F, Hagglund S, Bushlya V et al (2014) Influence of the minimum chip thickness on the obtained surface roughness during turning operations. Procedia CIRP 13:67–71
25. Rahman MA, Amrun MR, Rahman M et al (2016) Variation of surface generation mechanisms in ultra-precision machining due to relative tool sharpness (RTS) and material properties. Int J Mach Tools Manuf 115:15–28
26. Wojciechowski S, Twardowski P, Pelic M et al (2016) Precision surface characterization for finish cylindrical milling with dynamic tool displacements model. Precis Eng 46:158–165
27. Wojciechowski S, Maruda RW, Nieslony P et al (2016) Investigation on the edge forces in ball end milling of hardened steel. Int J Mech Sci 119:360–369
28. Zhu K, Lin X, Li K et al (2015) Compressive sensing and sparse decomposition in precision machining process monitoring: from theory to applications. Mechatronics 31:3–15
29. Wojciechowski S, Twardowski P, Wieczorowski M (2014) Surface texture analysis after ball end milling with various surface inclination of hardened steel. Metrol Meas Syst 21(1):145–156
30. Gadelmawla ES, Koura MM, Maksoud TMA et al (2002) Roughness parameters. J Mater Process Technol 123(1):133–145